Density of states for vibrations of fractal drums

Steven Homolya,* Charles F. Osborne, and Imants D. Svalbe
School of Physics and Materials Engineering, Monash University, Wellington Road, Clayton, Victoria 3800, Australia
(Received 5 August 2002; published 19 February 2003)

Vibrations of membranes with fractal boundaries (fractal drums) are investigated. Numerical results are presented for Koch drums of fractal dimension $D_f = 3/2$ at prefractal generations 1–3, and for Koch snowflake drums ($D_f = \ln 4/\ln 3$) at generations 3 and 4. The results show that the low-frequency integrated densities of states (IDOS's) of the drums are well approximated by a two-term asymptotic of the form given by the modified Weyl-Berry (MWB) conjecture, which predicts a correction of $\Delta N(\Omega) \propto \Omega^{D_f}$ to the leading-order Weyl term. In the high-frequency regime, where the half wavelength is smaller than the smallest features of the prefractal perimeter, the two-term Weyl asymptotic is applicable, with $\Delta N(\Omega) \sim \Omega$. The results also indicate that oscillations in $\Delta N(\Omega)$ arise due to localization of the wave amplitude near the prefractal perimeter. It is argued that for a self-similar fractal boundary, the amplitude of the oscillations is asymptotically proportional to Ω^{D_f}, which implies an $O(\Omega^{D_f})$, rather than the conjectured $o(\Omega^{D_f})$, error term for the asymptotic IDOS given by the MWB conjecture.

DOI: 10.1103/PhysRevE.67.026211 PACS number(s): 05.45.Df

I. INTRODUCTION

Fractal geometry provides a unifying theoretical framework for the description of natural irregularity [1]. The essential properties of hierarchically disordered systems are often determined by a single parameter, the fractal dimension. When different systems with the same fractal dimension display quantitatively similar behaviors, deterministic fractal models may be used to gain insight into the behavior of more complex naturally disordered systems [2]. In the present study, we consider vibrations of membranes with fractal boundaries, so-called fractal drums.

The natural modes ψ and frequencies ω of a drum are solutions of the Dirichlet boundary value problem,

$$(\nabla^2 + \omega^2)\psi = 0 \quad \text{on } S, \tag{1}$$

$$\psi = 0 \quad \text{on } \partial S, \tag{2}$$

where S and ∂S denote the planar surface and the boundary of the drum, respectively. Let $N(\Omega)$ denote the number of linear independent solutions ψ of Eqs. (1) and (2) with $\omega < \Omega$, i.e., the number of natural frequencies of the membrane (including degeneracies) less than Ω. The quantity $N(\Omega)$ is the integrated density of states (IDOS) of the system.

How $N(\Omega)$ depends on the geometry of the boundary is closely related to Kac's question "Can one hear the shape of a drum?" [3]. The Berry conjecture [4], and its modified form, the modified Weyl-Berry (MWB) conjecture, is that one can at least hear the fractal dimension of the boundary of a fractal drum, because the asymptotic, large Ω, IDOS follows

$$N(\Omega) = A_S\Omega^2/4\pi - C\Omega^{D_f} + o(\Omega^{D_f}), \tag{3}$$

where D_f is the fractal dimension of ∂S, A_S is the area of S, and C is a positive constant.

The Berry conjecture [4], where D_f is defined as the Hausdorff dimension, was disproved by counterexample in Ref. [5], where Brossard and Carmona suggested that the Minkowski dimension might be more appropriate. In Ref. [6], Lapidus showed that for a drum with Minkowski measurable perimeter ∂S, the following relation holds for large Ω:

$$\Delta N(\Omega) = A_S\Omega^2/4\pi - N(\Omega) \tag{4}$$

$$= O(\Omega^{D_f}), \tag{5}$$

where D_f is the Minkowski dimension of ∂S. Thus Lapidus proposed the MWB conjecture, with the value of the constant C in Eq. (3) also given a new interpretation. Later, Lapidus [7] showed that C cannot depend on the geometry of the perimeter in as simple a way as proposed in Ref. [6]. References [8,9] show that for some systems, the MWB conjecture cannot hold unless the constant C is replaced by a function of Ω that is oscillatory about a constant.

In Ref. [4], Berry proposed that his conjecture should also apply to prefractal systems in the low-frequency regime. References [10–17] considered resonators with the Koch curve boundary shown, for the third generation, in Fig. 1(a). The ranges of frequencies considered in Refs. [10–14] were insufficient for quantitative confirmation of the MWB conjecture. Nevertheless, the results indicated qualitative agreement, with the low-frequency modal density depleted by the irregularity of the perimeter. Hobiki, Yakubo, and Nakayama [15–17] computed the IDOS's of prefractal drums over a sufficiently broad range of frequencies, but obtained the curious result that the MWB conjecture is valid only in the high-frequency, short-wavelength, limit. The present study shows these conclusions to be incorrect.

*Electronic address: Steven.Homolya@spme.monash.edu.au

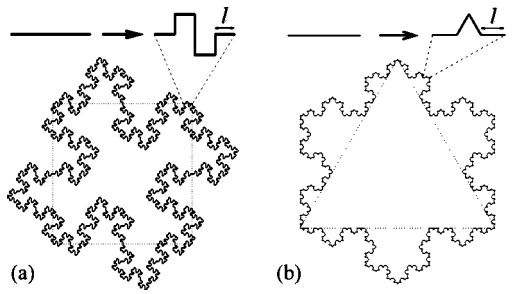

FIG. 1. Prefractal closed contours: (a) third-generation Koch curve, (b) fourth-generation Koch snowflake. The initiators are shown with dotted lines. The generators are shown above each contour. l denotes the length of the smallest line segments on each contour.

Reference [9] also includes numerical results for a Koch snowflake prefractal [Fig. 1(b)] aimed at confirming that C in Eq. (3) is an oscillatory function of Ω. The results showed that if C is the sum of a constant and an oscillatory term, the latter must be small compared with the former, perhaps zero.

In the present study, we examine the vibrations of several prefractal Koch drums by numerical computation of the natural modes and frequencies. The outline of the paper is as follows.

Section II revisits the physical argument that led to the formulation of Berry's conjecture for the IDOS's of fractal resonators, and consider what the same argument implies about the IDOS's of prefractal systems. The numerical method used to compute the vibrational modes of prefractal drums is described in Sec. III. Numerical errors are discussed in Secs. III C and III D. Numerical results for Koch drums with $D_f=1.5$ are presented in Sec. IV A, where we examine the origin of oscillations in the IDOS and their implications for fully fractal drums. Results for the Koch snowflake drum are included in Sec. IV B. In Sec. IV C, we argue that for self-similar fractal drums, localization of the wave amplitude by the fractal perimeter will always result in oscillations in the IDOS that can only be accommodated by Eq. (3) if C is oscillatory about a constant, with finite amplitude in the asymptotic limit. We summarize the main conclusions of the paper in Sec. V.

II. MODAL DENSITY FOR FRACTAL AND PREFRACTAL DRUMS

The asymptotic, large Ω, IDOS of a drum with a perimeter ∂S of finite length $a_{\partial S}$ is given by the Weyl formula:

$$N(\Omega)=A_S\Omega^2/4\pi-a_{\partial S}\Omega/4\pi+o(\Omega). \tag{6}$$

The first term on the right-hand side of Eq. (6) represents one state per area π^2/A_S in wave-vector space, due to the finite area of the drum. The second term is a small correction to this due to constraints imposed on the wave amplitude by the fixed boundary conditions. If ∂S is a fractal, then $a_{\partial S}$ is undefined and Eq. (6) is inapplicable.

Berry's proposition [4] may be stated as follows: A mode with a wavelength $\lambda=2\pi/\omega$ is largely unaffected by details of the perimeter whose sizes are of the order of a half wavelength $\lambda/2$ or smaller [23]. This may be quantified by replacing $a_{\partial S}$ in the Weyl formula [Eq. (6)] with an effective perimeter length that is a function of the frequency, for example, as measured using a caliper whose length is of the order of $\lambda/2=\pi/\omega$, at a frequency of $\omega=\Omega$. Thus

$$a_{\partial S}\rightarrow B\lambda^{1-D_f}=B(2\pi/\Omega)^{1-D_f}, \tag{7}$$

with B constant. Then, the second term in the modified Weyl formula becomes

$$-[B(2\pi)^{-D_f/2}]\Omega^{D_f}=-C\Omega^{D_f},$$

and we obtain Eq. (3).

If the perimeter is a prefractal with hierarchic structure over a finite range of length scales ($\gtrsim l$), then the substitution given by Eq. (7) may still be applicable at half wavelengths $\lambda/2\gtrsim l$, i.e., $\Omega\lesssim\pi/l$. At shorter wavelengths, the full length $a_{\partial S}$ of the perimeter becomes apparent, so the Weyl formula should be correct. We can summarize this by writing

$$\Delta N(\Omega)=\begin{cases} C\Omega^{D_f} & \text{for } \Omega\lesssim\pi/l \\ a_{\partial S}\Omega/4\pi & \text{for } \Omega\gtrsim\pi/l, \end{cases} \tag{8}$$

which is Berry's conjecture for the prefractal drum. Because Eq. (6) and its modified form [Eq. (3)] describe asymptotic behavior, relation $\Delta N\propto\Omega^{D_f}$ can only be relevant for the prefractal if there are a sufficiently large number of modes in the low-frequency regime, $\Omega\lesssim\pi/l$. To leading order in Ω, this may be expressed as $N(\pi/l)\approx A_S(\pi/l)^2/4\pi\gg 1$, i.e., $l^2\ll A_S$. This implies what is intuitively obvious, i.e., the hierarchic structure should be present over a sufficiently broad range of length scales, if the prefractal is to exhibit any of the characteristics (in this case modal density) of the fractal.

III. NUMERICAL METHOD

Numerical solutions of Eqs. (1) and (2) were obtained by discretizing S on a periodic mesh that is compatible with the prefractal boundary ∂S. The numerical method used here is a special case of that used to compute modes of inhomogeneous membranes in Ref. [18]. A summary of the method follows.

The value of the wave amplitude ψ is considered at a finite number of sites of a periodic lattice. The behavior of the function ψ is approximated using polynomial interpolation. Boundary conditions are included in the discrete model by imposing appropriate constraints on the interpolating polynomials. In the resulting approximation, the Laplacian in Eq. (1) is approximated by a sparse real symmetric matrix, and the wave amplitude by a column vector of sampled values of ψ. Eigenvalues and eigenvectors of the matrix correspond to the numerical approximations to solutions ω^2 and ψ, respectively, of the continuum problem defined by Eqs. (1) and (2). The matrix eigenvalue problem is solved efficiently using the Lanczos algorithm [19].

A more detailed discussion of the numerical method is given in the following sections.

TABLE I. Coefficients used to estimate the second-order partial derivatives of a sampled function ψ in Eq. (9).

M	C_1	C_2	C_3	C_4
1	1			
2	4/3	−1/12		
3	3/2	−3/20	1/90	
4	8/5	−1/5	8/315	−1/560

A. Approximating the Laplacian

We begin by imposing a periodic grid in the plane of the drum surface S. Let $f(u)$ denote the wave amplitude $\psi(\mathbf{r})$ along a grid line in the direction of a vector $\mathbf{a}$. For example, for a grid line through the origin, we let $f(u)=\psi(u\hat{\mathbf{a}})$, where $\hat{\mathbf{a}}=\mathbf{a}/|\mathbf{a}|$. Let the magnitude $a=|\mathbf{a}|$ of vector $\mathbf{a}$ correspond to the grid spacing, with grid points at $\mathbf{r}=n\mathbf{a}$, where n is an integer. The second-order partial derivative of $\psi(\mathbf{r})$ in the direction of $\mathbf{a}$ is approximated in an order-$2M$ scheme as

$$\partial^2_{\hat{\mathbf{a}}}\psi=\hat{\mathbf{a}}\cdot[\boldsymbol{\nabla}(\hat{\mathbf{a}}\cdot\boldsymbol{\nabla}\psi)]_{\mathbf{r}=n\mathbf{a}}=f''(u)|_{u=na}=\frac{1}{a^2}\sum_{m=1}^{M}C_m(f_{n+m}-2f_n+f_{n-m})+O(a^{2M}), \tag{9}$$

where $f_n=f(na)=\psi(n\mathbf{a})$ denote sampled values of $\psi(\mathbf{r})$ along the grid, and C_m are constants that depend on M only. Equation (9) may be obtained by interpolating sampled values, $f_{n-M},\ldots,f_{n+M}$, of f by a polynomial of degree $2M$, or by expanding $f(u)$ as a Taylor series about $u=na$. The values of constants C_m are shown in Table I for $M=1$–4. For $M=1$, Eq. (9) reduces to the second-order central-difference scheme used in Refs. [9–17]. For $M=2$, Eq. (9) is equivalent to the fourth-order improved scheme as discussed in Ref. [20].

For a triangular grid, each grid point is the intersection of three grid lines, along vectors $\mathbf{a}_j$, $j\in\{1,2,3\}$, as shown in Fig. 2. The Laplacian of ψ may be expressed as a linear combination of second-order partial derivatives $\partial^2_{\hat{\mathbf{a}}_j}\psi$ along the grid lines:

$$\nabla^2\psi=\sum_{j=1}^{3}\alpha_j\partial^2_{\hat{\mathbf{a}}_j}\psi \tag{10}$$

with

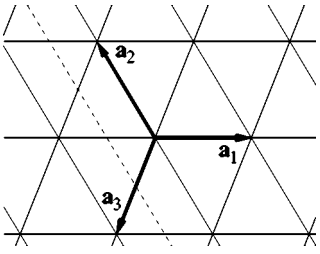

FIG. 2. Triangular mesh defined by vectors $\mathbf{a}_1$, $\mathbf{a}_2$, and $\mathbf{a}_3$. The dashed line is an example of where a boundary may be placed in the discrete representation of a drum's surface. (See Sec. III B.)

$$\alpha_j=\left|\epsilon_{jlm}a_j^2\frac{\mathbf{a}_l\cdot\mathbf{a}_m}{(\mathbf{a}_j\times\mathbf{a}_l)\cdot(\mathbf{a}_j\times\mathbf{a}_m)}\right|, \tag{11}$$

where ϵ_{jlm} is the permutation symbol and $a_j=|\mathbf{a}_j|$. For a hexagonal lattice with $p6m$ symmetry, we have $a_1=a_2=a_3$ and $\alpha_j=2/3$. For a square lattice, say with $\mathbf{a}_1\perp\mathbf{a}_2$ and $a_1=a_2$, we get $\alpha_1=\alpha_2=1$ and $\alpha_3=0$, as long as the grid is not singular, i.e., no two of $\mathbf{a}_j$ are parallel. The lattice approximation of $\nabla^2\psi$ is obtained by replacing partial derivatives on the right-hand side of Eq. (10) by the order-$2M$ approximation given by Eq. (9) for $\mathbf{a}=\mathbf{a}_j$. When this is done at every lattice site, Eq. (1) is approximated by a matrix eigenvalue problem of the form

$$\sum_m L_{mn}\psi_m=\omega^2\psi_n, \tag{12}$$

where ψ_m denote the sampled values of the wave amplitude ψ, and coefficients L_{mn} are derived from the discrete approximations of partial derivatives given by Eq. (9). Neglecting boundary conditions for the moment, the form of Eq. (9) guarantees that, for given M, L_{mn} depends only on $|m-n|$, so the matrix $[L_{mn}]$ is real and symmetric. The matrix is also sparse, since, at each lattice site, only a few nearest neighbor sites are considered ($4M$ neighbors for a rectangular mesh, and $6M$ neighbors for a triangular mesh). These properties of $[L_{mn}]$ make the eigenproblem of Eq. (12) suitable for efficient solution using the Lanczos algorithm [19].

B. Boundary conditions

Let us suppose that there is a fixed boundary at $\mathbf{r}=0.5\mathbf{a}$, between lattice sites at $\mathbf{r}=0$ on the exterior and at $\mathbf{r}=\mathbf{a}$ on the interior of S. Function $f(u)=\psi(n\mathbf{a})$ is therefore defined for $u>0.5a$. The domain of the function $f(u)$ may be extended to $u\leqslant 0.5a$, in a manner consistent with fixed boundary conditions, by requiring that $f(u)$ be an odd function of $(u-0.5a)$. This corresponds to setting

$$f_{-m+1}=-f_m,\quad m\geqslant 1. \tag{13}$$

Using Eq. (13), we can define boundaries that bisect straight line segments connecting nearest neighbor lattice points, as indicated by the dashed line in Fig. 2. The advantage of this, compared with having fixed boundary sites, as in Refs. [12,13], is that the same lattice model can be used for both fixed and free boundary systems. For a free boundary, the minus sign on the right hand side of Eq. (13) is omitted.

To allow efficient solution of Eq. (12), the symmetry of the matrix of coefficients L_{mn} must be retained after boundary conditions are imposed. We can confirm this by substituting Eq. (13) in Eq. (9), which, after rearranging, gives

$$f''(u)|_{u=na}=\frac{1}{a^2}\sum_m(C_{|m-n|}-C_{n+m-1})f_m,$$

where summation is over all $m\geqslant 1$, and we have defined $C_0=-2\Sigma_{m=1}^{M}C_m$ and $C_{m>M}=0$.

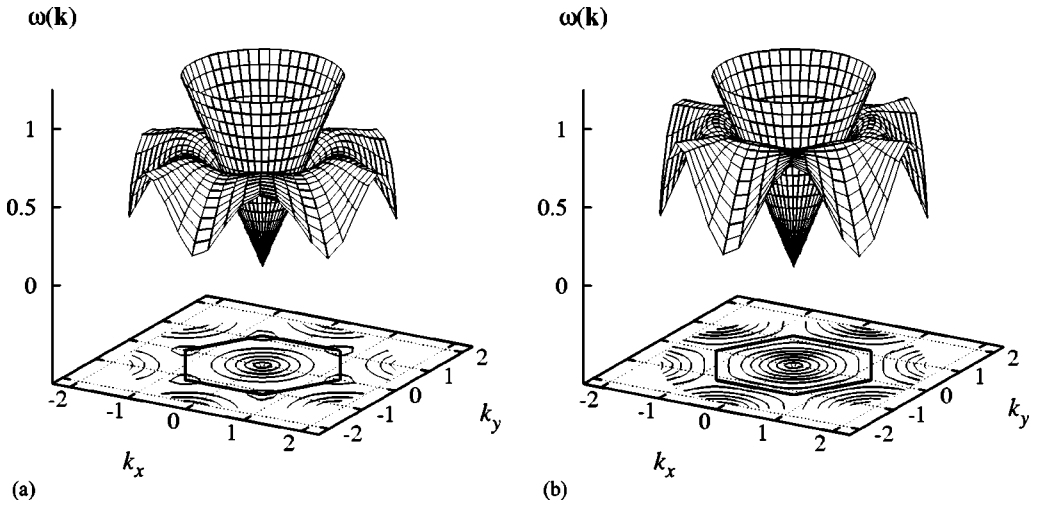

FIG. 3. Dispersion relations for a hexagonal lattice model of a membrane using (a) second-order and (b) eighth-order interpolation. The angular frequency ω, and the wave-vector components, k_x and k_y, are expressed in units of π/a, with a denoting the lattice constant. The boundary of the first Brillouin zone of the lattice is indicated by the thick solid lines at the base of each plot. The linear dispersion relation is signified by the $\omega=|\mathbf{k}|$ cones.

C. Nonlinear dispersion

Previous numerical studies on prefractal resonators employed the second-order central-difference method and considered the accuracy of ''trivial'' eigenvalues of the drum as indicators of the accuracy of the scheme in general [10,13,15]. For the Koch drum, as shown in Fig. 1(a), trivial modes arise from the tilability of the drum surface by squares of area, l^2. Frequencies of the square drum of area l^2 are also frequencies of the Koch drum. The accuracy of the lattice model for these modes may be assessed by considering plane wave solutions of Eq. (1):

$$\psi(\mathbf{r})=e^{i\mathbf{k}\cdot\mathbf{r}} \tag{14}$$

with

$$\omega^2=|\mathbf{k}|^2. \tag{15}$$

Considering Eqs. (9) and (10), for the lattice model, the linear dispersion relation [Eq. (15)] is replaced by

$$\omega^2=4\sum_{m=1}^{M}\sum_{j=1}^{3}\frac{C_m\alpha_j}{a_j^2}\sin^2(m\mathbf{k}\cdot\mathbf{a}_j/2) \tag{16}$$

$$=|\mathbf{k}|^2\left[1+\sum_{j=1}^{3}O(|\mathbf{k}\cdot\mathbf{a}_j|^{2N})\right]. \tag{17}$$

The periodicity of ω as a function of $\mathbf{k}$ is a direct consequence of the discrete nature of the model system. All unique traveling wave solutions are contained in the first Brillouin zone of the lattice.

In Fig. 3, we have plotted the frequency ω against the wave vector $\mathbf{k}$, for second- and eighth-order schemes ($N=1,4$, respectively) employing a hexagonal lattice with $\mathbf{a}_1=a\hat{\mathbf{x}}$, $|\mathbf{a}_1|=|\mathbf{a}_2|=|\mathbf{a}_3|=a$ and $\mathbf{a}_1+\mathbf{a}_2+\mathbf{a}_3=0$. The $\omega=|\mathbf{k}|$ cones correspond to the linear dispersion relation characteristic of the continuous medium. Figure 3 shows that compared with the second-order central-difference method [Fig. 3(a)], the higher-order scheme [Fig. 3(b)] provides a better approximation of the continuous system. This is most evident at larger values of $|\mathbf{k}|$ in the first Brillouin zone of the lattice, signified by the thick solid lines at the base of each plot. The lattice dispersion relations show anisotropy, reflecting the $p6m$ symmetry of the grid. Analogous statements apply for the square lattice.

We define the error ε in the numerical approximation as the relative error in frequencies ω_{apx} of the lattice system compared with the frequencies ω_{xct} of the continuum:

$$\varepsilon=|\omega_{\mathrm{xct}}-\omega_{\mathrm{apx}}|/\omega_{\mathrm{xct}}. \tag{18}$$

Figure 4 shows ε as a function of ak/π, for plane waves on a square lattice. Errors are shown for second- to eighth-order schemes. The data show that higher-order schemes do perform better. For a given value of $|\mathbf{k}|=k\leqslant\pi/a$, the error in ω is reduced by increasing the order $2M$ of the approximation on the same grid. This also implies that using a higher-order scheme and a coarser grid (larger a), we can achieve the same accuracy as with a lower-order scheme and a finer grid. This is of practical importance, since it allows more efficient use of computational resources.

D. Boundary effects

The presence of a boundary introduces further errors in the lattice approximation of the drum surface. The difficulty in extending the above analysis to a bound system arises from a fundamental difference between the continuum problem and its discrete counterpart. For the continuum problem, we can consider eigenstates of the Laplacian operator, from which we select those that satisfy boundary conditions. For the lattice, boundary conditions are accommodated by modifying the discrete approximation of the Laplacian. One con-

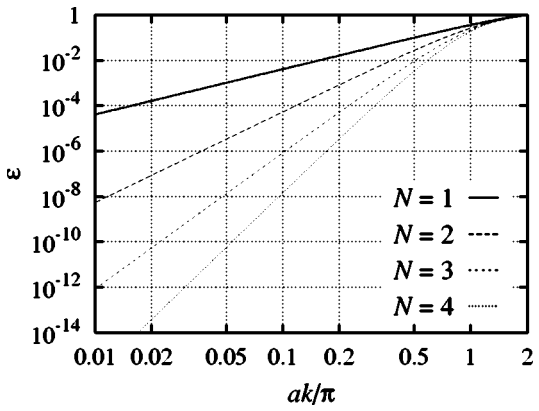

FIG. 4. Relative errors ε in frequencies of plane waves approximated by order-$2M$ interpolations on a square lattice, plotted as a function of ak/π. The quantity $k=|\mathbf{k}|$ is the wave number and a is the lattice constant. The error ε depends on both the magnitude k and the direction of the wave vector, because of lattice anisotropy. For given k, ε is greatest when $\mathbf{k}$ is parallel with one of the two orthogonal lattice vectors. The errors shown here correspond to this case.

sequence of this is that plane waves are not eigenstates of the bound lattice Laplacian, so the relevance of Eq. (16) is questionable. Trivial modes of the Koch drum are a special case where, in a plane wave decomposition, boundary terms happen to cancel exactly. It is reasonable to assume that the presence of a boundary will, in general, increase errors in the approximation, so Eq. (16) indicates the best result we can expect from the numerical model.

Errors in the frequencies of a drum computed using the lattice model may be estimated numerically from the dependence of the numerical solution on grid size. We have examined this for the second generation $D_f=1.5$ Koch drum. The surface of the drum was discretized using a square grid, with the length l of the smallest boundary segment stretching over an integral number n of lattice constants $a=l/n$. A larger n value corresponds to a higher resolution grid and therefore a more detailed discrete representation of the drum surface. The first 2000 distinct frequencies were computed for $n=2,3,\ldots,20$. Here we show one typical example.

Figure 5(a) shows the numerical approximations to the 1000th distinct frequency. Plots of ω against n are shown for second- and eighth-order interpolations ($M=1,4$). As expected, for both schemes, the frequency appears to approach a constant value, $\omega=\omega_{\mathrm{xct}}$, for large n. Figure 5(a) indicates that the higher-order scheme provides a better approximation for given n. Extrapolating the $N=4$ data set, by assuming a power law dependence of the error ε on n at large n, we estimate $\omega_{\mathrm{xct}}=(137.38\pm0.01)\sqrt{A_S}$. From this, we have estimated the relative error ε, which is plotted in Fig. 5(b) as a function of grid spacing a. The ranges of values of ε, given by the dispersion relation [Eq. (16)] for square lattices, are indicated by the dotted curves. [For given M, there is a range of errors because of lattice anisotropy. The upper and lower bounds for ε are obtained from Eq. (16) applied to the square lattice with the wave vector $\mathbf{k}$ parallel with and at 45° to grid lines, respectively.] Errors for the second-order scheme are

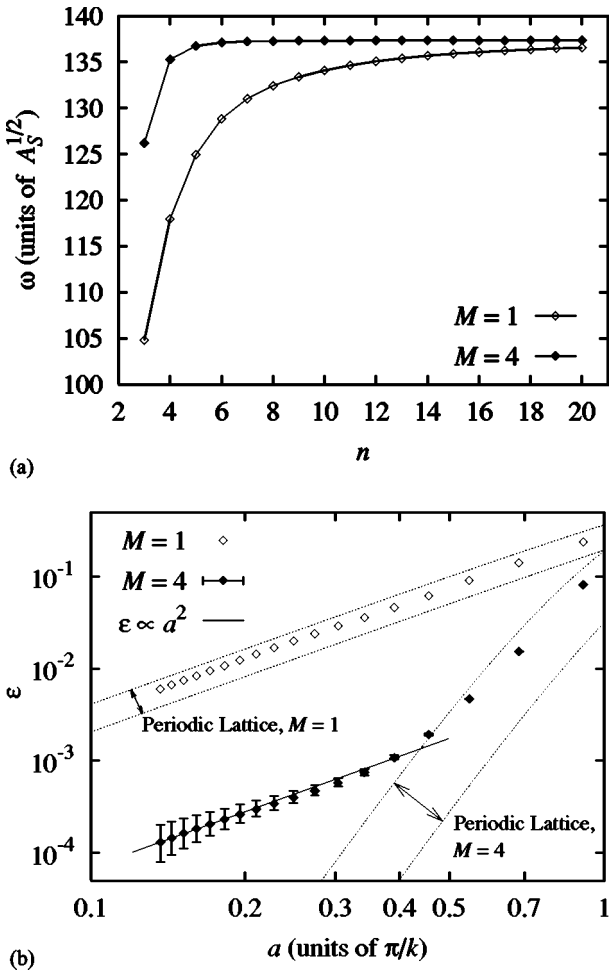

FIG. 5. Convergence of numerical solution for the 1000th distinct frequency ω of the second generation Koch drum of area A_S. (a) Plot of ω against number of grid points n per characteristic length l. (b) Plot of relative error ε in frequency against lattice constant a. Results are shown for second- and eighth-order discrete models ($M=1$ and 4, respectively).

within this range for all a considered. For the eighth-order approximation, the lattice dispersion relation gives a good indication of the error for low resolution grids, $ak/\pi\gtrsim0.5$, i.e., $4a\gtrsim\lambda$. For $4a\lesssim\lambda$, the rate of convergence of the $M=4$ solution slows to about $\varepsilon=O(a^2)$. In this region, errors for $M=4$ remain about 1.5 orders of magnitude smaller than errors for $M=1$. It would appear that, for the higher-order scheme, $O(a^{2M})$ errors on the interior of the lattice dominate for large a (coarse grid) and lower-order errors associated with boundary conditions dominate for small a (fine grid).

Numerical results presented in Sec. IV were obtained using lattice approximations with $M=4$, and the computed frequencies ω correspond to $ak/\pi<0.25$. The example shown in Fig. 5 indicates better than three digits of precision for ω in this range. We note that the accuracy of the eighth-order lattice model is reduced by up to an order of magnitude compared with the example shown here, for modes where the wave amplitude is strongly localized near the boundary of the system. However, the number of such modes is small, less than 1% of the number of frequencies computed.

E. Mode count and degeneracy

To determine the mode count $N(\Omega)$ from eigenvalues $\omega^2<\Omega^2$, the degeneracy of each eigenvalue is required. The Lanczos algorithm used to solve Eq. (12) cannot determine the degeneracies without the expensive computation of all eigenvectors [19], p. 155]. To compute the modal density over a greater range of frequencies than this procedure would allow, the number of essential degeneracies was estimated by writing Eqs. (1) and (2) in a form that explicitly includes the symmetry of *S*. This shows that for the Koch drums with $C4$ and $C6M$ symmetries [Figs. 1(a) and 1(b), respectively], one in three and one in two distinct eigenvalues can be expected to be twofold degenerate, respectively.

Hence, the IDOS $N(\Omega)$ may be estimated by

$$N(\Omega)\simeq\gamma N_{\mathrm{dis}}(\Omega)+\delta N_{\mathrm{acc}}(\Omega), \tag{19}$$

where $\gamma=4/3$, 3/2 for the $C4$ and $C6M$ symmetries, respectively, $N_{\mathrm{dis}}(\Omega)$ is the number of distinct eigenvalues $\omega^2<\Omega^2$, and $\delta N_{\mathrm{acc}}(\Omega)$ denotes any further contribution from accidental degeneracies. Taking into account known ''accidental'' degeneracies of trivial modes, Eq. (19) provided estimates within two counts of the actual IDOS, for the lattice models of generation $\nu=1,2$ drums, and also over the first 1000 frequencies for third generation drums. Equation (19) was used to obtain the results presented below for third- and fourth-generation drums.

IV. RESULTS AND DISCUSSION

To facilitate comparison between the modal densities of prefractal drums of different generations ν, we present the numerical results in terms of the scaled quantities

$$\Omega_{\mathrm{scl}}=\Omega l/\pi, \tag{20}$$

$$\Delta N_{\mathrm{scl}}=4l\Delta N/a_{\partial S}. \tag{21}$$

Ω_{scl} is the frequency expressed on a scale where $\Omega_{\mathrm{scl}}=1$ at $\lambda=2l$, and ΔN_{scl} is the IDOS correction term ΔN scaled by a generation-dependent factor of $4l/a_{\partial S}$. In terms of the scaled quantities, Eq. (8) may be written as

$$\Delta N_{\mathrm{scl}}(\Omega_{\mathrm{scl}})=\begin{cases} C'\Omega_{\mathrm{scl}}^{D_f}, & \Omega_{\mathrm{scl}}\lesssim 1 \\ \Omega_{\mathrm{scl}}, & \Omega_{\mathrm{scl}}\gtrsim 1, \end{cases} \tag{22}$$

where C' is a constant independent of the generation of the prefractal. Equation (22) follows from Eqs. (8), (20), (21), and from $a_{\partial S}\propto l^{1-D_f}$ for $A_S=\mathrm{const}$.

A. Koch drum, $D_f=1.5$

Drums and Neumann resonators with the $D_f=1.5$ Koch curve boundary, shown in Fig. 1(a) for generation $\nu=3$, were the subjects of Refs. [10–17]. The boundary of a generation ν drum consists of $4\times8^{\nu}$ straight line segments of length *l*, so the perimeter of the drum is $a_{\partial S}=4\times8^{\nu}l$ and the area is $A_S=4^{2\nu}l^2$. The fractal dimension is $D_f=\ln 8/\ln 4=1.5$. The natural frequencies of generation $\nu=1,2,3$ drums were computed using a square grid. Details of the numerical computations are summarized in Table II.

TABLE II. Details of computations for $D_f=1.5$ Koch drums. Columns show ν, prefractal generation number; l/a, number of lattice spacings per smallest perimeter segment length; number of degrees of freedom (DOF) of the numerical model; number of frequencies computed (including degeneracies); largest frequency computed (rounded to two significant figures).

ν	l/a	DOF	$\leqslant N$	$\lesssim\omega l/\pi$
1	40	160^2	750	8.0
2	20	320^2	5000	5.1
3	8	512^2	13333	2.1

1. IDOS: Overall structure

Figure 6 shows numerical results for $\Delta N_{\mathrm{scl}}(\Omega_{\mathrm{scl}})$, over a frequency range of $\Omega_{\mathrm{scl}}\leqslant 2.25$. This range includes all our results for the third-generation, $\nu=3$, Koch drum. For $\nu=1$ and 2, [Figs. 6(a) and 6(b), respectively] only part of the results are shown here to allow comparison between the three data sets. First, let us consider the low-frequency regime, $\Omega_{\mathrm{scl}}<1$, where the IDOS is conjectured to be affected by the hierarchic structure of the perimeter. For the first-generation drum [Fig. 6(a)], there are only five modes with frequencies in this range, which is insufficient to imitate the asymptotics of the IDOS of a fractal drum. For $\nu=2$ and 3 [Figs. 6(b) and 6(c), respectively], there are 136 and $\approx$2712 modes (2034 distinct frequencies) with $\Omega_{\mathrm{scl}}<1$, and the low-frequency IDOS shows good agreement with the conjectured $\Delta N_{\mathrm{scl}}\propto\Omega_{\mathrm{scl}}^{D_f}$ relation, particularly for $\Omega_{\mathrm{scl}}<0.87$. The relation is applicable for $\Omega_{\mathrm{scl}}<0.87$. At higher frequencies, the IDOS is better characterized by the ordinary Weyl asymptotic, $\Delta N_{\mathrm{scl}}=\Omega_{\mathrm{scl}}$. However, there are significant deviations about this overall trend. These deviations are remarkably similar for different generation prefractals. We return to discuss the reason for this in Sec. IV A 2, but first let us examine the IDOS's of the first- and second-generation drums, over the full range of the computed frequencies. The results are shown in Fig. 7. The $\nu=1$ data are shown as points and the $\nu=2$ data as a thick solid curve. The high-frequency IDOS's of both drums are clearly oscillatory about the Weyl asymptotics, which is signified by the dashed line. The oscillations are similar in character for the two sets of results, and show quasiperiodicity with a period of unity in Ω_{scl}.

The results suggest that the overall structure of the spectrum persists from one prefractal generation to the next. For example, $\Delta N_{\mathrm{scl}}(\Omega_{\mathrm{scl}})$ for $\nu=2$ [Fig. 6(b)] is a good approximation to $\Delta N_{\mathrm{scl}}(\Omega_{\mathrm{scl}})$ for $\nu=3$ [Fig. 6(c)], except for the finest structures and at the lowest frequencies. The same comments apply to the $\nu=1,2$ results (Fig. 7). In Fig. 8, we have plotted IDOS's of the three drums on one set of logarithmic axes. The results clearly show good agreement with Eq. (22). Least squares fits of $\ln(\Delta N_{\mathrm{scl}})=X\ln\Omega_{\mathrm{scl}}+\mathrm{const}$, over $\Omega_{\mathrm{scl}}\leqslant 0.87$, give $X=1.473\pm0.002$ for $\nu=3$, and $X=1.51\pm0.01$ for $\nu=2$, in good agreement with the conjectured $X=D_f=1.5$. The errors in X are the asymptotic stan-

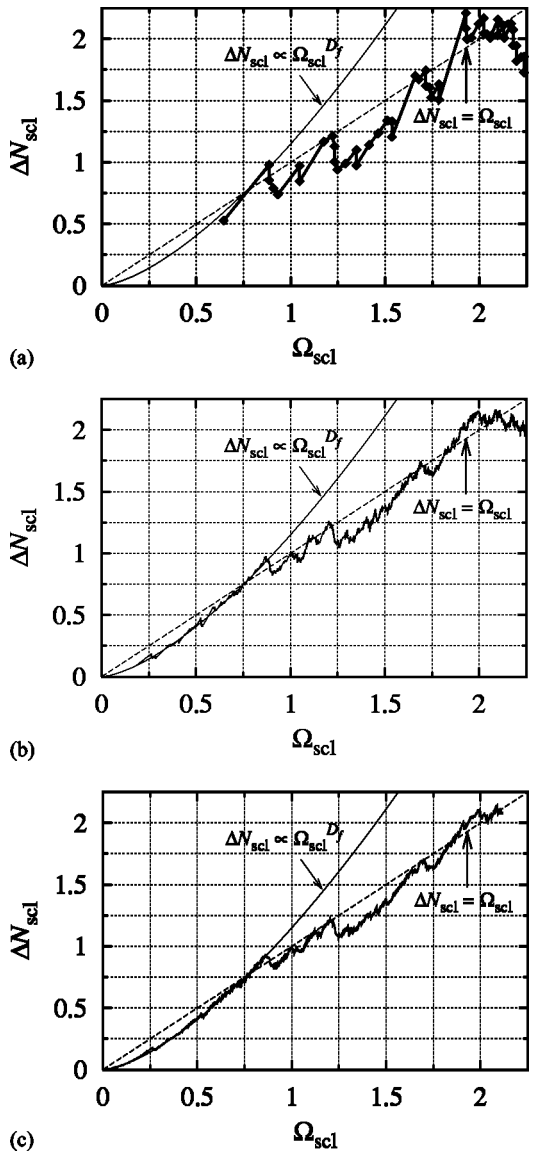

FIG. 6. Numerical results for the low-frequency scaled IDOS correction term $\Delta N_{\mathrm{scl}}(\Omega_{\mathrm{scl}})$, for Koch drums of generation (a) $\nu=1$, (b) $\nu=2$, and (c) $\nu=3$.

dard errors for the fits. At higher frequencies $\Omega_{\mathrm{scl}} \gtrsim 0.87$, the MWB conjecture is clearly inapplicable, and the IDOS follows $\Delta N_{\mathrm{scl}}(\Omega_{\mathrm{scl}}) = \Omega_{\mathrm{scl}}$, as expected for a perimeter of finite length. (See Ref. [8], and references therein.)

2. IDOS: Fine structure

The results in Figs. 6–8 show that the IDOS's of the prefractal drums exhibit significant oscillations. The oscillations show hierarchic structure, with smaller oscillations within larger ones. This is illustrated in Fig. 9, which shows the fluctuation $\Delta N_{\mathrm{scl}}/\Omega_{\mathrm{scl}}$ of ΔN_{scl} about the Weyl asymptotic $\Delta N_{\mathrm{scl}} = \Omega_{\mathrm{scl}}$, on several scales. The results indicate that the number of levels of hierarchy for oscillations in the IDOS increases with prefractal generation ν. A quantitative analysis of the relationship between the hierarchic structure of the spectrum and the hierarchic geometry of the system will be given elsewhere. In the present study, we concentrate on the general implications of the persistence of fine structure in the spectrum, from one prefractal generation to the next, as illustrated in Figs. 6, 7, and 9.

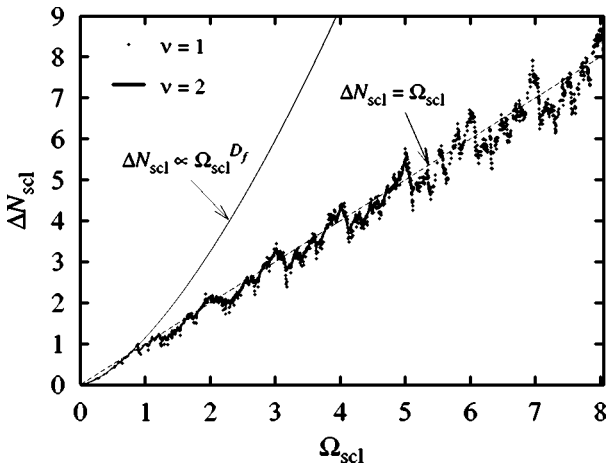

FIG. 7. Numerical results for the scaled IDOS correction term $\Delta N_{\mathrm{scl}}(\Omega_{\mathrm{scl}})$, for Koch drums of generation $\nu=1$ and 2. Results are shown for the full range of computed frequencies.

Peaks in modal density occur at approximately the same frequencies (in units of π/l) for different generation drums. A region of high modal density corresponds to a decrease in $\Delta N(\Omega)$ with increasing Ω. The origin of the peaks in modal density becomes apparent after examining the corresponding modes of the drums. As an example, let us consider modes in the frequency range $0.87 < \Omega l/\pi < 0.90$, where an increase in modal density signals the end of the range of applicability of the MWB conjecture [Eq. (3)]. For many of the modes in this frequency range, the wave amplitude is localized near the perimeter, in *T*-shaped subdomains of the drum. An example is shown in Fig. 10(a), for $\nu=2$. The modes are quasidegenerate, with frequencies close to that of the fundamental, $\omega = 0.909\pi/l$, of a *T*-shaped membrane of area $4l^2$.

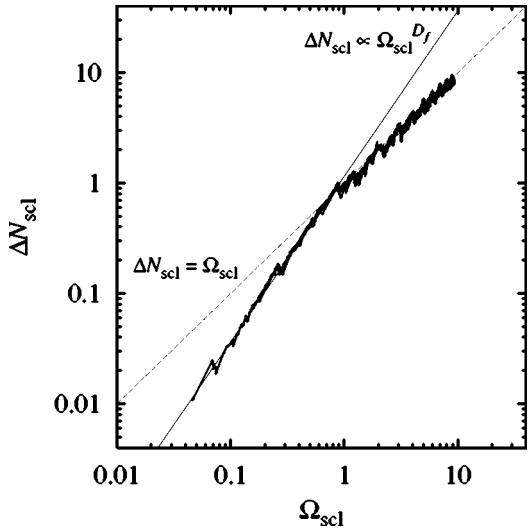

FIG. 8. Pooled numerical results for $\Delta N_{\mathrm{scl}}(\Omega_{\mathrm{scl}})$ of generation 1–3 prefractal Koch drums.

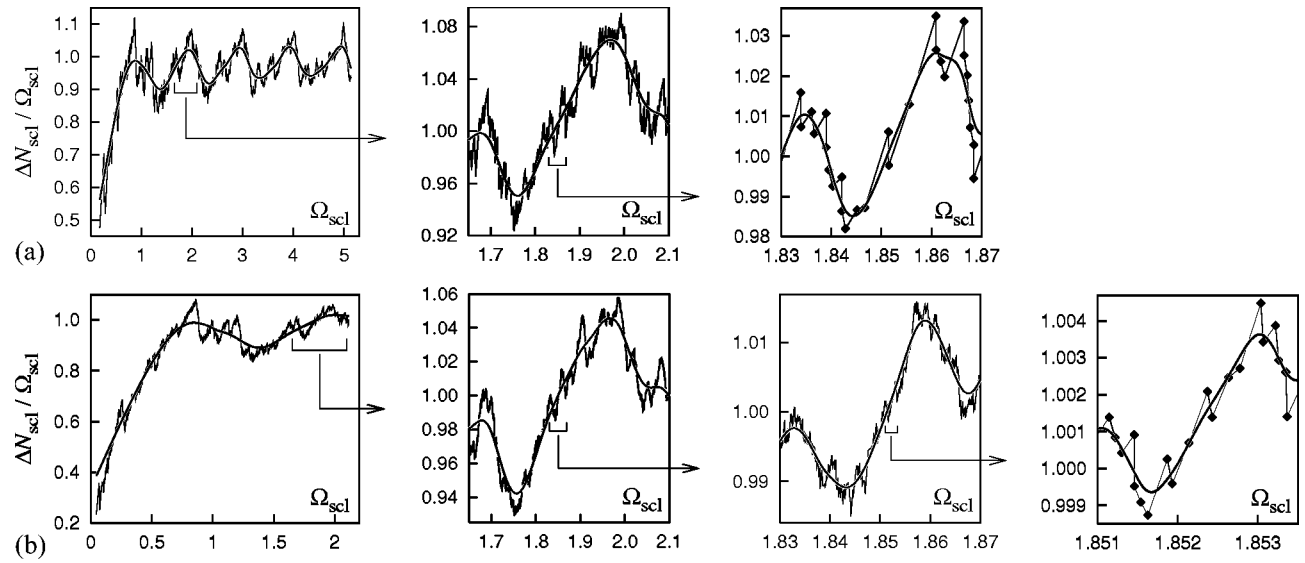

FIG. 9. Plots of the fluctuation $\Delta N_{\rm scl}/\Omega_{\rm scl}$ of the scaled IDOS correction term $\Delta N_{\rm scl}$, about the Weyl asymptotic, $\Delta N_{\rm scl}=\Omega_{\rm scl}$. The graphs illustrate the hierarchy of oscillations in the IDOS of generation (a) $\nu=2$ and (b) $\nu=3$ Koch drums. The smooth curves are cubic splines fitted to the data. In the last graph of (a), the data points correspond to numerical results for eigenfrequencies of the drum, including degeneracies. In the last graph of (b), the data points represent distinct frequencies, with the IDOS approximated by Eq. (19).

For the Koch drums, there is an accumulation of modes near this frequency. Accumulation of states, due to localization near the prefractal perimeter, has been previously proposed to be exclusive to Neumann systems, where the boundaries are free to move [15]. Our results indicate that the mechanisms responsible for localization and fluctuations in modal density have similar origins in both fixed and free boundary systems.

The most prominent peaks in the IDOS occur at frequencies that are approximately integral multiples of π/l, i.e., near $\Omega_{\rm scl}\in\mathbb{N}$. (See Figs. 7 and 9.) At these frequencies, localized standing waves of wavelengths $\lambda\simeq 2l/n$, $n\in\mathbb{N}$, are set up in $l\times l$ square regions at the perimeter. Figure 10(b) shows an example for $\nu=2$, at $\omega\simeq 3\pi/l$.

Some of the small enclosed regions near the boundary [Figs. 11(a)–11(c)] are clearly related to the most prominent oscillations of the IDOS. These regions are present for all generations $\nu\geqslant 1$, which explains why the IDOS's of different generation drums are qualitatively similar. For higher generation drums, larger (in units of l) regions on ∂S [such as those shown in Figs. 11(d) and 11(e)] result in clusters of fewer frequencies, and smaller oscillations in $\Delta N(\Omega)$. (See Fig. 9.)

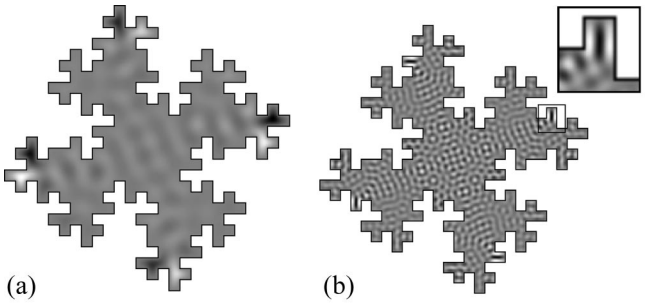

FIG. 10. Localized modes of the second-generation Koch drum at frequencies of (a) $\omega=0.88\pi/l$, (b) $\omega=3.01\pi/l$. Black and white represent maximum amplitudes, with displacements of opposing signs.

(a) Prefractal generation dependence. The numerical results indicate that high modal density regions of the spectrum may be related to multiple instances of a geometric pattern on the perimeter ∂S. For Koch drums of generations $\nu\leqslant 3$, we can identify at least five distinct patterns that are responsible for much of the fine structure of the spectra. These are shown in Fig. 11, with examples of associated modal displacements. For a repeating pattern P on ∂S to cause a strong accumulation of modes, it must partially enclose a subdomain of the drum that is relatively well separated from the rest of the drum's surface, by being connected to it through a narrow channel. This geometry will aid localization in the small peninsula enclosed by P. When the coupling between the peninsula and the ''mainland'' is sufficiently weak, the natural frequencies of the peninsula will show up, weakly perturbed, in the spectrum of the entire system. Each frequency should occur as many times as the number of instances of the peninsula. If there are n_P instances of P on ∂S, then we can expect to find n_P-fold quasidegeneracies near some of the natural frequencies of the peninsula.

For the pattern shown in Fig. 11(d), there are $n_P=4$ instances for generation $\nu=2$, and $n_P=16$ for $\nu=3$. There are strongly localized quasidegenerate modes associated with this contour at $\omega=0.524\pi/l$, with wave amplitudes as shown in Fig. 11(d). In Figs. 12(a) and 12(b), we have plotted, for $\nu=2$ and 3, respectively, the distinct frequency count $N_{\rm dis}$ against eigenfrequency ω, near $\omega=0.524\pi/l$.

For $\nu=2$ [Fig. 12(a)], three distinct frequencies occur in a narrow range. Numerical results for the modal displacement show that one of the three frequencies belongs to a degenerate mode. Hence, for $\nu=2$, there is a set of $n_P=4$ quasidegenerate modes associated with the open contour P of Fig.

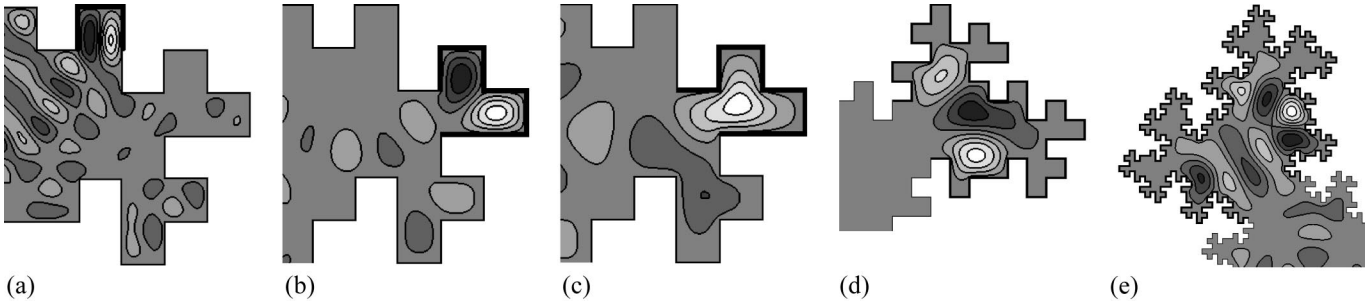

FIG. 11. Prefractal contours along the boundary, indicated by the thick lines, associated with localization and regions of high modal density in the spectra of generation 1–3 Koch drums. The contour plots, on the interiors of the drums, show the wave amplitude for examples of localized modes. Black and white represent maximum amplitudes, with displacements of opposing signs. Eigenfrequencies are $\omega=$(a) $2.12\pi/l$, (b) $1.23\pi/l$, (c) $0.885\pi/l$, (d) $0.524\pi/l$, (e) $0.231\pi/l$.

11(d). For $\nu=3$ [Fig. 12(b)], there are 12 distinct frequencies. Four can be expected to be degenerate because of symmetry, so there are $n_P=16$ frequencies in a range of width $1.63\times10^{-5}\pi/l$. This represents a modal density that is over 300 times (337 ± 2) greater than that expected from Eq. (3).

These clusters of quasidegenerate frequencies result in a steplike decrease in $\Delta N_{\rm scl}(\Omega_{\rm scl})$, over a narrow range of frequencies near $\Omega_{\rm scl}=0.524$. The height of the step is

$$H_P(\nu)\simeq 4l n_P(\nu)/a_{\partial S}=8^{-\nu}n_P(\nu). \tag{23}$$

Therefore, depending on whether $n_P(\nu)$ increases with ν faster or slower than 8^ν, $H_P(\nu)$ will increase or decrease, respectively, with increasing prefractal generation ν. For the above example, we have $n_P(3)=4n_P(2)$, so the size $H_P(\nu)$ of the drop in $\Delta N_{\rm scl}(\Omega_{\rm scl})$ at $\Omega_{\rm scl}=0.524$, is reduced by a factor of 2, as the generation of the drum is increased from 2 to 3.

For the patterns shown in Fig. 11, the ratio

$$r_P(\nu)=n_P(\nu)/n_P(\nu-1), \tag{24}$$

where defined, is less than 8 for $\nu\leqslant3$. This is consistent with the results shown in Figs. 6, 7, and 9, which show that the amplitudes of oscillations in $\Delta N_{\rm scl}(\Omega_{\rm scl})$ decrease with increasing ν. [Relation $r_P(\nu)<8$ is not universally true for any pattern P. For example, trivially, $r_P(\nu)=8$ for line segments of length l, and $r_P(2)=9$ for the curve P: ⌐┘, which consists of four segments of length l.]

The generation dependence of the quantity $n_P(\nu)$ may be used to infer about the amplitudes of oscillations in the IDOS's of higher generation drums. Because the number of straight line segments of length l on the prefractal perimeter increases eightfold from one generation to the next, we may expect that, for large ν,

$$n_P(\nu)\sim 8^\nu \quad \text{and} \quad r_P(\nu)\to 8, \tag{25}$$

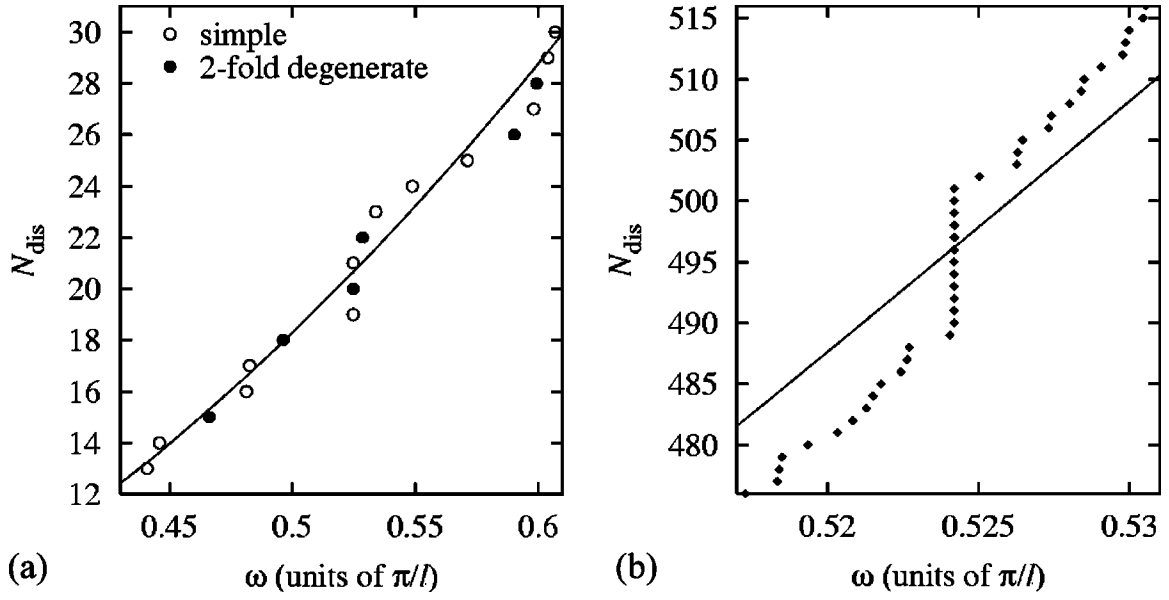

FIG. 12. Distinct frequency count $N_{\rm dis}$ plotted as a function of eigenfrequency ω, for generation (a) $\nu=2$ and (b) $\nu=3$ Koch drums, near the quasidegenerate frequency of $\omega=0.524\pi/l$. In (a), frequencies corresponding to doubly degenerate modes are signified by filled circles. The solid curves in both plots correspond to the MWB conjecture [Eq. (3)], with constant C obtained from a best fit to the low-frequency, $\Omega<0.87\pi/l$, IDOS $N(\Omega)$.

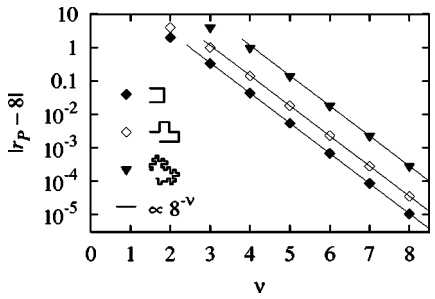

FIG. 13. Selected results for number of instances $n_p(\nu)$ of prefractal contours P (shown on the left) on the perimeters of generation ν prefractal Koch drums. The quantity plotted is $|r_P-8|$, where $r_P(\nu)$ is given by Eq. (24).

for any pattern P, unless $n_P(\nu)=0$ for all ν. By Eq. (23), this would imply finite $H_P(\nu)$ for all ν.

Equations (23) and (25) are specific to the Koch curve. However, similar relations apply to any self-similarly iterated curve. Suppose, the total number of length l line segments increases α-fold in increasing the generation number ν by 1. [For the Koch curve of Fig. 1(a), $\alpha=8$, and for the Koch snowflake of Fig. 1(b), $\alpha=4$.] Then the length of the perimeter follows $a_{\partial S}(\nu)\propto\alpha^{\nu}l$, and Eqs. (23) and (25) become $H_P(\nu)\simeq 4ln_P(\nu)/a_{\partial S}\propto\alpha^{-\nu}n_P(\nu)$ and $n_P(\nu)\sim\alpha^{\nu}, r_P(\nu)\to\alpha$, respectively, which still implies finite $H_P(\nu)$ for large ν.

To confirm Eq. (25) numerically, we have counted the number of instances $n_P(\nu)$ of repeating patterns P on higher generation, $\nu\leqslant 8$, prefractal contours, using the following method.

The prefractal closed contours ∂S are encoded as strings of characters that represent instructions for traversing the contour in the counterclockwise direction. Each character represents a change, or no change, in direction. A straight line segment of length l is assumed between each neighboring pair of characters. For example, the string *LLLL* (with periodic boundary conditions) represents a square, with *L* for "turn left 90°." A string representing a generation ν prefractal Koch curve is obtained by inserting the generator string *LRRSLLR* (*R* for right and *S* for straight) between neighboring characters in the generation $\nu-1$ string, starting with the initiator string *LLLL* for $\nu=0$. To count the number of instances $n_P(\nu)$ of a geometric pattern P on a prefractal contour F, we count the number of matches of P's representative string (e.g., *SLLRLLR* for P: ⏢) in F's string.

We have plotted $|r_P(\nu)-8|$ in Fig. 13, for a selection of patterns P. Similar results are obtained for all P considered. The results confirm Eq. (25). In all cases, r_P rapidly approaches the asymptotic value of 8, with

$$|r_P(\nu)-8|\sim 8^{-\nu}, \tag{26}$$

or $r_P(\nu)=8$, where defined. Equation (26) implies that for any P, the quantity $H_P(\nu)$ approaches a finite constant value $H_P(\infty)$ for large ν, with

$$H_P(\nu)-H_P(\infty)\sim 8^{-\nu}.$$

TABLE III. Details of numerical computations of eigenfrequencies of Koch snowflake prefractal drums. Definitions of column headings are given in Table II.

ν	l/a	DOF	$\leqslant N$	$\lesssim \omega l/\pi$
3	16.5	142849	6000	4.0
4	7.5	290893	15000	2.1

Therefore, the oscillations we observe in the IDOS's of the generation $\nu\leqslant 3$ prefractals persist with a finite amplitude for all $\nu>3$. In the IDOS's of higher generation drums, still smaller oscillations should arise from localization in subdomains of the drum surface, which are larger (in units of l) than those shown in Fig. 11. These will contribute smaller but finite amplitude oscillations in $\Delta N_{\rm scl}(\Omega_{\rm scl})$ for arbitrarily large ν.

(b) Fractal limit. In the fractal limit ($\nu\to\infty$), regions that facilitate localization will exist at arbitrarily small length scales. Because the boundary ∂S is a self-similar iterated set, for a fractal contour P_0 on ∂S that partially encloses a small (size s_0) region of the drum surface, there will also be smaller, geometrically similar, contours P_μ on ∂S, which partially enclose similar regions of sizes $s_\mu=s_0\alpha^{-\mu/D_f}$, $\forall\,\mu\in\mathbb{N}$, where α is the constant that characterizes how the fractal scales. The number of instances n_μ of contours P_μ on the perimeter ∂S follows

$$n_\mu\sim s_\mu^{-D_f} \quad \text{for} \quad s_\mu\to 0, \quad \mu\to\infty, \tag{27}$$

by definition of D_f as the self-similarity dimension. If P_0 facilitates localization at a wavelength of λ_0, then there will be a cluster of n_0 modes at a frequency of $\omega=\Omega_0=2\pi/\lambda_0$. Since P_0 is geometrically similar to all P_μ, there will also be modes localized in all regions congruent with P_μ, at wavelengths $\lambda_\mu=(s_\mu/s_0)\lambda_0$. This implies clusters of n_μ modes at frequencies $\omega=\Omega_\mu=2\pi(s_0/s_\mu)/\lambda_0$. Then by Eq. (27), we have

$$n_\mu\sim\Omega_\mu^{D_f} \text{ for } \Omega_\mu\to\infty. \tag{28}$$

The IDOS $N(\Omega)$ of the fractal drum will increase abruptly by $n_\mu\sim\Omega^{D_f}$ counts at $\Omega=\Omega_\mu$, because of n_μ-fold quasidegeneracies at frequencies $\omega=\Omega_\mu$. This implies finite asymptotic fluctuations in the correction [Eq. (4)] to the Weyl leading term, i.e.,

$$\Delta N(\Omega)-C\Omega^{D_f}=O(\Omega^{D_f}), \quad \forall\ \ C\in\mathbb{R}, \tag{29}$$

contrary to Eq. (3), which would imply

$$\Delta N(\Omega)-C\Omega^{D_f}=o(\Omega^{D_f}), \quad \exists\ \ C\in\mathbb{R}.$$

B. Koch snowflake

To support the above conclusions, we also computed the frequency spectra of Koch snowflake boundary drums. The fourth-generation boundary is shown in Fig. 1(b). For generation ν, the perimeter consists of $3\times 4^{\nu}$ segments of length

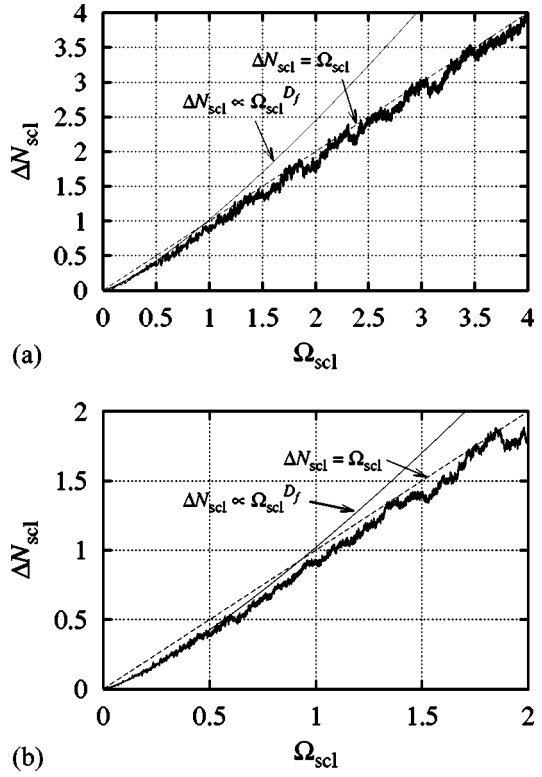

FIG. 14. Numerical results for $\Delta N_{\mathrm{scl}}(\Omega_{\mathrm{scl}})$ of generation (a) $\nu=3$ and (b) $\nu=4$ Koch snowflake boundary drums.

l, with $a_{\partial S}=3\times 4^4 l$ and $A_S=\sqrt{3}l^2(8\times 9^\nu-3\times 4^\nu)/20$. The fractal dimension is $D_f=\ln 4/\ln 3\simeq 1.2619$.

The drums were discretized using a hexagonal lattice. Here, we present results for drums of generations $\nu=3$ and 4. Details of the numerical computations are shown in Table III.

The numerical results for $\Delta N_{\mathrm{scl}}(\Omega_{\mathrm{scl}})$ are shown in Fig. 14. In the low-frequency regime, $\Omega_{\mathrm{scl}}\lesssim 0.45$, the data show good agreement with the conjectured $\Delta N\propto\Omega^{D_f}$ relation. At high frequencies, $\Omega\gtrsim\pi/l$, the IDOS is again better characterized as oscillatory about the Weyl asymptotic, $\Delta N(\Omega)\propto\Omega$. In Fig. 15, the two sets of data are plotted on logarithmic axes. Best fits of $\ln(\Delta N_{\mathrm{scl}})=X\ln\Omega_{\mathrm{scl}}+\mathrm{const}$ over $\Omega_{\mathrm{scl}}\leqslant 0.45$ give $X=1.28\pm 0.01$ for $\nu=4$, and $X=1.3\pm 0.1$ for $\nu=3$, in good agreement with the conjectured $X=D_f\simeq 1.26$. Data points involving the lowest frequencies, $N_{\mathrm{dis}}\leqslant 10$ ($\Omega_{\mathrm{scl}}<0.082$ for $\nu=4$ and $\Omega_{\mathrm{scl}}<0.244$ for $\nu=3$), were considered to be outliers and were excluded from the fit.

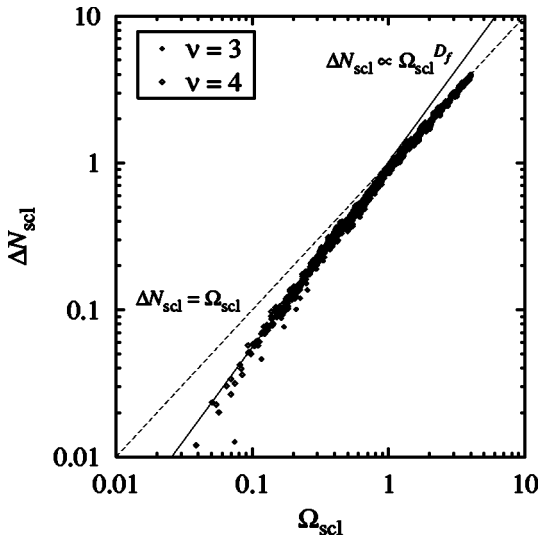

FIG. 15. Log-log plot of numerical results for $\Delta N_{\mathrm{scl}}(\Omega_{\mathrm{scl}})$ of Koch snowflake boundary drums of generations $\nu=3$ and 4.

Figure 14 shows that oscillations in the IDOS of the Koch snowflake drum persist from one generation to the next, in much the same way as they persist for the $D_f=1.5$ Koch drum (Fig. 6). However, for the snowflake drums, the modal density does not have narrow peaks that might be easily identified with quasidegeneracies and localized modes. This may be attributed to differences in the geometries of the boundaries of the $D_f=1.5$ drums and the snowflake drums. Unlike the $D_f=1.5$ Koch curve, the snowflake boundary does not facilitate narrow channels between different regions of the drum surface, which could give rise to well-defined peninsulas and strongly localized modes.

Numerical results show that localization does still occur near the boundary, albeit to a lesser extent than in the $D_f=1.5$ Koch drums. Figure 16(a) shows an example of a mode of the third-generation drum, at a frequency of $\omega\simeq 0.36\pi/l$. The wave amplitude is partially localized in the six largest lobes of the drum. For $\nu=3$, there are six modes that are localized in a similar way, though they do not contribute a significant increase to the modal density. For $\nu=4$, there are 18 similar subdomains of the boundary, where localization may occur in the same way. Two examples of the corresponding modes are shown in Figs. 16(b) and 16(c). The distinct frequency count N_{dis} is plotted against frequency ω in Fig. 16(d), showing that, for $\nu=4$, there is a significant increase in modal density, near $\omega=0.36\pi/l$. However, this is a relatively weak accumulation of modes, compared with those observed for the $D_f=1.5$ drums, as, for example, in Fig. 12(b). In the following section, we argue that even this weak accumulation of modes implies greater fluctuation, $O(\Omega^{D_f-2})$, in the IDOS of the fractal, than predicted by the MWB conjecture, $o(\Omega^{D_f-2})$.

C. Fluctuations in the DOS for a self-similar boundary

Let us assume that near some frequency Ω_μ, the modal density of the fractal is enhanced by localization near the boundary, so that the DOS $\rho(\Omega)$ near $\Omega=\Omega_\mu$ is

$$\rho(\Omega_\mu)=\rho_{\mathrm{MWB}}(\Omega_\mu)+\delta\rho_\mu, \tag{30}$$

where ρ_{MWB} is the DOS given by the MWB conjecture and $\delta\rho_\mu$ represents the enhancement due to accumulation of localized modes. ρ_{MWB} is obtained, by differentiating the IDOS given by Eq. (3), as

$$\rho_{\mathrm{MWB}}(\Omega)=A_S\Omega/2\pi-D_f C\Omega^{D_f-1}+o(\Omega^{D_f-1}). \tag{31}$$

Let us further suppose that the enhancement $\delta\rho_\mu$ is attribut-

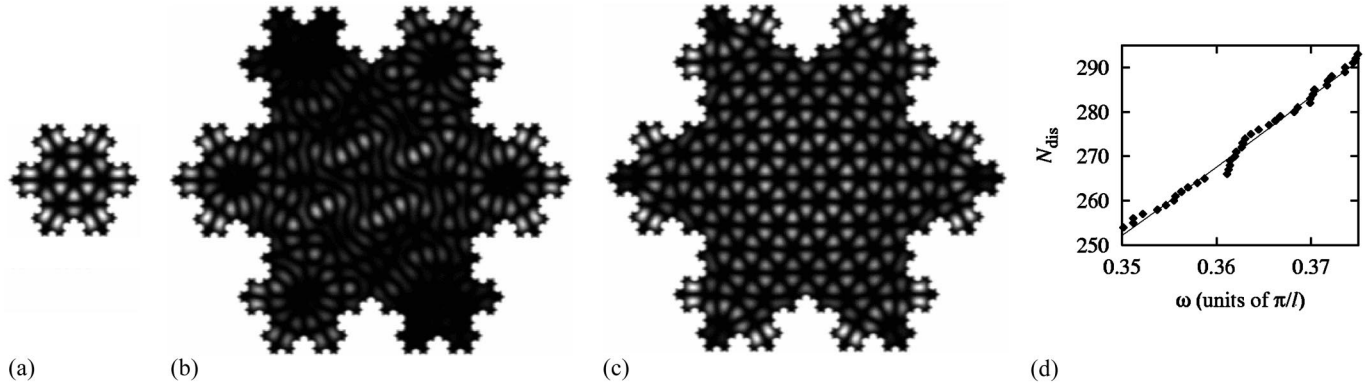

FIG. 16. Localized modes of generation (a) $\nu=3$ and (b), (c) $\nu=4$ Koch snowflake drums, at frequencies near $\omega=0.36\pi/l$. To aid visualization, the square of the modal displacement $|\psi|^2$ is shown, rather than ψ. Black and white correspond to zero and maximum amplitudes, respectively. (d) shows a plot of the distinct frequency count N_{dis} against eigenfrequency ω, for the $\nu=4$ drum, near the frequencies of the localized modes: $\omega=$(a) $0.357\pi/l$, (b) $0.363\pi/l$, (c) $0.3644\pi/l$.

able to n_μ modes localized in n_μ similar regions at the fractal boundary, with frequencies in a range of width $\Delta\Omega_\mu$ centered on $\omega=\Omega_\mu$. Then

$$\delta\rho_\mu \simeq n_\mu/\Delta\Omega_\mu .$$

Because of self-similarity, there will be localized modes at frequencies $\Omega_\mu=\alpha^{\mu/D_f}\Omega_0$, $\forall\mu\in\mathbb{N}$, with α constant. For large μ and Ω_μ, the width $\Delta\Omega_\mu$ of the interval, containing the n_μ localized modes near $\omega\approx\Omega_\mu$, cannot be greater than $O(\Omega_\mu)$. Then by Eq. (28), $\delta\rho_\mu$ must be at least $O(\Omega_\mu^{D_f-1})$. The rigorous result of Eq. (5) implies that, for $\Omega\to\infty$,

$$A_S\Omega/2\pi-\rho(\Omega)=O(\Omega^{D_f-1}),$$

so $\delta\rho_\mu$ cannot be greater than $O(\Omega_\mu^{D_f-1})$ either. Therefore, we must have $\delta\rho_\mu\sim\Omega^{D_f-1}$ (and $\Delta\Omega_\mu\sim\Omega_\mu$). This is consistent with our earlier result [Eq. (29)], which was obtained by assuming that $\Delta\Omega_\mu$ is negligible. The $\delta\rho_\mu\sim\Omega_\mu^{D_f-1}$ term in Eq. (30) represents local enhancements of the DOS at $\ln\Omega=\mu\ln\alpha+\ln\Omega_0$, for integral μ, which supports the idea that the constant C in Eq. (3) should be replaced by a periodic function of $\ln\Omega$ [8].

The numerical results for the IDOS of the third-generation $D_f=1.5$ prefractal Koch drum show precursors to the periodicity of the fluctuations in the IDOS of the fractal drum. Notably, Fig. 8 shows that the most prominent peaks in the low-frequency DOS of the prefractal are at $\Omega l/\pi=\Omega_{\mathrm{scl}}=0.074,0.27,0.89$, i.e., $\ln(\Omega_{\mathrm{scl}})\approx-2.6,-1.3,-0.1$.

V. SUMMARY AND CONCLUDING REMARKS

We have investigated the harmonic vibrations of membranes with prefractal Koch curve boundaries, using a spatially discrete numerical model. The accuracy of the numerical method was assessed by reference to exactly solvable cases involving plane waves, as well as by examining the dependence of the numerical approximation, for frequencies of a Koch drum, on the spatial resolution of the discrete model. Numerical results for the natural frequencies of prefractal drums show that the low-frequency integrated densities of states (IDOS's) are well approximated by a two-term expression of the form given by the modified Weyl-Berry (MWB) conjecture [Eq. (3)]. At high frequencies, where the half wavelength is smaller than the smallest features of the drum perimeter, the IDOS $N(\Omega)$ oscillates about the two-term Weyl asymptotic [Eq. (6)] that characterizes smooth, nonfractal, boundary systems.

Numerical results for the normal modes of prefractal drums show that oscillations in the IDOS, in both the low- and high-frequency regimes, are due to localization of the wave amplitude near the prefractal perimeter. We have argued that the scaling properties of the perimeter imply that oscillations in the IDOS of a finite generation prefractal drum will persist, with finite amplitudes, for arbitrarily high generations. The IDOS's of high generation prefractal drums can be approximated by the IDOS of a lower generation drum, except for the finest structures of the spectra. This was confirmed numerically for Koch drums of generations 1–3, and for Koch snowflake drums of generations 3 and 4.

For fractal drums, ''trapped'' modes near the self-similar perimeter will cause oscillations in the IDOS $N(\Omega)$ with amplitudes $\sim\Omega^{D_f}$. These oscillations are superimposed on the asymptotic IDOS given by the MWB conjecture, and are not accounted for by the $o(\Omega^{D_f})$ error term. Instead, the error term should be $O(\Omega^{D_f})$, which reduces Eq. (3) to the rigorous result of Eq. (5). Our results indicate that Eq. (3) might be valid if the constant C is replaced by a periodic function of $\ln\Omega$, as suggested in Ref. [8].

Although these conclusions indicate that the MWB conjecture cannot be rigorous, the numerical results show that oscillations in the IDOS's of the Koch drums are small, and the two-term asymptotic given by Eq. (3) is a good practical approximation. In this study, we have considered only fixed boundary, Dirichlet, systems. For free, Neumann, boundary conditions, the MWB conjecture is identical to Eq. (3), except that the constant C is negative. Numerical results in Refs. [15,16] indicate that localization and associated mode accumulation arise in a similar way in Neumann and Dirichlet systems.

The numerical results of Refs. [15,16], for a Neumann

resonator with a second generation Koch curve boundary, suggest that oscillations in the IDOS of a fractal resonator with a free boundary are much greater than for the same resonator with a fixed boundary. This is because a free boundary supports more localized modes than a fixed boundary. For a Neumann fractal, the amplitude of oscillations in the IDOS may be comparable to the magnitude of the second term in Eq. (3), so the MWB conjecture may not be a good approximation to the IDOS, beyond the leading-order Weyl term. We plan to compute the spectra of higher generation prefractal Neumann resonators in detail, to investigate the differences between vibrations in free and fixed boundary fractals.

For fractals, the $O(\Omega^{D_f})$ oscillatory component of the IDOS is a direct consequence of the exact self-similarity of the boundary. For a random fractal, the oscillations in the asymptotic IDOS may be suppressed, or even absent. For example, a natural enclosure, such as a cave with irregular walls [21], might have a much smoother frequency response for sound waves than a concert hall with prefractal walls that are composed of geometrically similar building blocks. The fractal resonator problem may turn out to be an example of a physical system where, unlike in many other cases [2], random and deterministic fractality produce markedly different behaviors.

ACKNOWLEDGMENTS

S.H. acknowledges the financial support of the Australian Government through the Australian Postgraduate Awards Scheme. Computations were performed at the HPC facilities of the Victorian Partnership of Advanced Computing [22].

[1] B. B. Mandelbrot, *The Fractal Geometry of Nature* (W. H. Freeman, New York, 1983).
[2] M. Filoche and B. Sapoval, Phys. Rev. Lett. **84**, 5776 (2000), and references therein.
[3] M. Kac, Am. Math. Monthly **73**, 1 (1966).
[4] M. V. Berry, in *Structural Stability in Physics* edited by W. Güttinger and H. Eikemeier (Springer-Verlag, Berlin, 1979), pp. 51–53. URL: http://www.phy.bris.ac.uk/research/theory/Berry/the_papers/Berry082.pdf
[5] J. Brossard and R. Carmona, Commun. Math. Phys. **104**, 103 (1986).
[6] M. L. Lapidus, Trans. Am. Math. Soc. **325**, 465 (1991).
[7] M. L. Lapidus, Math. Proc. Cambridge Philos. Soc. **119**, 167 (1996).
[8] M. Levitin and D. Vassiliev, Proc. London Math. Soc. **72**, 188 (1996).
[9] J. Fleckinger, M. Levitin, and D. Vassiliev, Proc. London Math. Soc. **71**, 372 (1995).
[10] B. Sapoval, Th. Gobron, and A. Margolina, Phys. Rev. Lett. **67**, 2974 (1991).
[11] B. Sapoval and Th. Gobron, Phys. Rev. E **47**, 3013 (1993).
[12] S. Russ, B. Sapoval, and O. Haeberlé, Phys. Rev. E **55**, 1413 (1997).
[13] B. Sapoval, O. Haeberlé, and S. Russ, J. Acoust. Soc. Am. **102**, 2014 (1997).
[14] C. Even *et al.*, Phys. Rev. Lett. **83**, 726 (1999).
[15] Y. Hobiki, K. Yakubo, and T. Nakayama, Phys. Rev. E **52**, R1310 (1995).
[16] Y. Hokiki, K. Yakubo, and T. Nakayama, Physica B **219–220**, 354 (1996).
[17] Y. Hobiki, K. Yakubo, and T. Nakayama, Phys. Rev. E **54**, 1997 (1996).
[18] S. Homolya, I. D. Svalbe, and C. F. Osborne, J. Sound Vib. (to be published).
[19] J. K. Cullum and R. A. Willoughby, *Lanczos Algorithms for Large Symmetric Eigenvalue Computations* (Birkhuser, Boston, 1985), Vol. 1.
[20] R. Szilard, *Theory and Practice of Plates: Classical and Numerical Methods* (Prentice-Hall, London, 1974), p. 184.
[21] A. P. Radliński *et al.*, Phys. Rev. Lett. **82**, 3078 (1999).
[22] See the VPAC Home Page at http://www.vpac.org/
[23] In Ref. [4], Berry assumed that details smaller than λ are unimportant. Here we use $\lambda/2$ as the approximate cutoff, which leads to the same result for a fractal.